

# Muffin Tin Orbitals of Arbitrary Order

O.K. Andersen and T. Saha-Dasgupta

*Max-Planck-Institut für Festkörperforschung, Postfach 800665, D-70506 Stuttgart, Germany*

(October 24, 2018)

## Abstract

We have derived orbital basis sets from scattering theory. They are expressed as polynomial approximations to the energy dependence of a set of partial waves, in quantized form. The corresponding matrices, as well as the Hamiltonian and overlap matrices, are specified by the values on the energy mesh of the screened resolvent and its first energy derivative. These orbitals are a generalization of the 3rd-generation linear MTOs and should be useful for electronic-structure calculations in general.

For electrons in condensed matter, it is often desirable to express the one-electron wave functions,  $\Psi_i(\mathbf{r})$ , with energies,  $\varepsilon_i$ , in a certain range in terms of a *minimal set* of energy-independent orbitals,  $\chi_{RL}(\mathbf{r})$ . Here,  $R$  labels sites and  $L$  the local symmetry (e.g.  $L \equiv lm$ ).

The simplest example of such an orbital is the Wannier function,  $\chi(\mathbf{r} - \mathbf{R})$ , for an isolated band. A more realistic example is illustrated in Fig. 1, the conduction-band orbital of a cuprate high-temperature superconductor. This orbital is centered on Cu, has anti-bonding  $O_x p_x - \text{Cu } d_{x^2-y^2} - O_y p_y$  character, and extends beyond the 3rd-nearest neighbor atoms. Its Bloch sum describes a tight-binding (TB) band:  $\varepsilon_{\mathbf{k}} \sim \langle \varepsilon \rangle - 2t(\cos k_x + \cos k_y) + 4t' \cos k_x \cos k_y - 2t''(\cos 2k_x + \cos 2k_y)$ . This orbital is the starting point for descriptions of the low-energy physics of the cuprates. Its is *not* a Wannier function. First of all because the conduction band is merely one partner of a bonding, non-bonding, anti-bonding triple with nearly degenerate Cu  $d$  and O  $p$  levels so that the three bands nearly stick together at  $\varepsilon_p \sim \varepsilon_d$  with a cone-like behavior at the centre of the zone. As a result, the true Wannier function of the anti-bonding band has very long range, but since  $\varepsilon_p \sim \varepsilon_d$  is 2–3 eV below the Fermi level, the low-energy physics is hardly influenced by this. The second reason why the orbital of interest cannot be a Wannier function, is that the conduction band is crossed by, or has avoided crossings with other bands (Fig. 2). Since this occurs an eV below  $\varepsilon_F$ , this, too, is irrelevant for the low-energy physics, which should therefore be described using an orbital which yields correct wave functions at and near  $\varepsilon_F$  and has errors  $\propto (\varepsilon_i - \varepsilon_F)^{N+1}$ . The wider the energy range described correctly by this orbital, *i.e.* the higher the  $N$ , the longer its spatial range.

We have found a *general* method, the NMTO method, by which for instance this kind of orbital can be obtained [1]. What Fig. 1 shows is in fact a muffin-tin orbital (MTO) with  $N=1$ , obtained from a density-functional (DF-LDA) NMTO calculation. This method has recently enabled us to compute how the hopping integrals  $t$ ,  $t'$ , and  $t''$  are influenced by chemical and structural factors, and it has proved successful for computing  $t_{\parallel}$  and  $t_{\perp}$  for the ladder cuprates without resort to the common, but dubious procedure of fitting to guessed TB bands [3].

In Fig. 2 we demonstrate that a *single* MTO of sufficiently high  $N$  is capable of describing the *entire* conduction band, including its cone-like feature as well as smooth interpolations across avoided crossings: The dotted band was obtained variationally using an MTO with  $N=3$ , thus yielding band-errors of order  $2(N+1)=8$ . This figure also demonstrates that one may use a *discrete* mesh of energies,  $\epsilon_0, \dots, \epsilon_N$ , to construct the MTO, which then has errors  $\propto (\epsilon_i - \epsilon_0) \dots (\epsilon_i - \epsilon_N)$ . This is analogous to using Lagrange or Newton interpolation instead of Taylor expansion, and is far more practical. The band obtained variationally has errors  $\propto (\epsilon_i - \epsilon_0)^2 \dots (\epsilon_i - \epsilon_N)^2$ .

For some purposes, it is better to use a larger set of more localized orbitals. For instance, in order to understand the microscopic origins of  $t$ ,  $t'$ , and  $t''$ , we used a set with Cu  $d_{x^2-y^2}$ , O  $p_x$ , O  $p_y$ , and Cu  $s$ , obtained by upfolding through a screening transformation [1,4,5].

Materials with *many* bands and strong correlations are being studied intensively. The first step of a quantitative description is a one-electron mean-field theory requiring a basis, flexible enough to give individual orbitals desired properties. For this, NMTOs are uniquely suited.

As an example of a minimal set spanning all states in a *wide* energy range, let us consider the LDA valence and conduction bands for GaAs, 18 of which fall in the range between -15 and +20 eV. With a Ga  $sp^3d^5$  As  $sp^3d^5f^7$  basis of merely 25  $N=2$  MTOs per GaAs, and mesh points at -15, 0, and 10 eV, we obtained a variational band structure, which only above +15 eV yielded errors as large as 0.1 eV. Even for this 35 eV-range, which includes the Ga 3d semi-core band at -15 eV, *no* principal quantum numbers were needed. To most practitioners, this is surprising result. NMTOs should be useful for computing excited-state properties with the GW method [7].

For ground-state properties, only the Ga 3d and the valence bands must be described. Using the minimal Ga  $sp^3d^5$  As  $sp^3$  MTO set, we find accuracies in the sum of the one-electron energies of 50 and 5 meV per GaAs for respectively  $N=1$  and  $N=2$  [1]. This is highly satisfactory and opens the way for accurate and efficient DF-calculations, for instance for large systems using techniques where the computation increases merely linearly with the

size of the system. Hitherto, this has only been possible with less accurate or geometry-restricted methods [2,6], such as semi-empirical TB, screened LMTO-ASA [4], or screened multiple-scattering theory [8].

The LMTOs of the 1st- and 2nd-generations [4] were expressed in terms of partial waves,  $\varphi_{Rl}(\epsilon_0, r_R) Y_L(\hat{r}_R)$ , and their energy derivatives,  $\dot{\varphi}_{Rl}(\epsilon_0, r_R) Y_L(\hat{r}_R)$ , truncated outside the atomic spheres ( $r_R \equiv |\mathbf{r} - \mathbf{R}|$ ). Everything else was neglected in the atomic-spheres approximation (ASA), which then gave rise to a simple formalism and fast computation. The 3rd-generation [5] succeeds in making this formalism valid for overlapping MT potentials,  $V(\mathbf{r}) = \sum_R v_R(r_R)$ , to first order in the overlap of the  $v$ 's, thus making the ASA superfluous. This is accomplished by attaching tails of screened spherical waves with the proper energy to the partial waves. The resulting set of *kinked* partial waves, evaluated on the energy mesh, is what the NMTO set is expressed in terms of:

$$\chi_{R'L'}^{(N)}(\mathbf{r}) = \sum_{n=0}^N \sum_{RL} \phi_{RL}(\epsilon_n, \mathbf{r}) L_{nRL, R'L'}^{(N)}. \quad (1)$$

This may be considered as a polynomial approximation to the energy dependence of the partial-wave set, in quantized form. In the following, we derive the expressions for the Lagrange matrices,  $L_n^{(N)}$ , and the NMTO Hamiltonian and overlap matrices, starting out from the conceptually simplest way of solving Schrödinger's equation, namely by matching of partial solutions. Our formalism should prove useful also in other contexts.

We consider the case where the wave functions  $\Psi_i(\mathbf{r})$  are solutions of a Schrödinger equation with a MT potential,  $\mathcal{H}\Psi_i(\mathbf{r}) \equiv [-\Delta + V(\mathbf{r})]\Psi_i(\mathbf{r}) = \epsilon_i\Psi_i(\mathbf{r})$ . For simplicity, we first assume that the MT wells do not overlap and have ranges,  $a_R$ . At the end, definitions will be modified in such a way that the formalism holds also for overlapping wells. The  $a$ 's will be hard-sphere radii which define the screening and, hence, the shape of the orbitals.

*Kinked partial waves* [5]. –Inside a MT sphere, the partial solutions factorize into energy-dependent radial functions,  $\varphi_{Rl}(\epsilon, r_R)$ , and angular functions. In the interstitial, we use screened spherical waves, which are defined as those solutions of the wave equation,  $(\Delta + \epsilon)\psi_{RL}(\epsilon, \mathbf{r}) = 0$ , which satisfy the homogeneous boundary condition that the projec-

tion of  $\psi_{RL}(\varepsilon, \mathbf{r})$  onto  $\delta(r_{R'} - a_{R'}) Y_{L'}(\hat{r}_{R'})$  be  $\delta_{RR'} \delta_{LL'}$ . In fact, only those solutions with  $RL$  corresponding to the so-called *active* channels will be used (in Fig. 1, the central Cu  $d_{x^2-y^2}$ ), and only the projections onto other *active* channels will vanish (all non-central Cu  $d_{x^2-y^2}$  projections). The projection of  $\psi_{RL}(\varepsilon, \mathbf{r})$  onto an *inactive* channel (all other than  $d_{x^2-y^2}$  on any Cu-sphere) satisfies the boundary condition that its radial logarithmic derivative equals that of the radial *Schrödinger*-solution. The kinked partial wave,  $\phi_{RL}(\varepsilon, \mathbf{r})$ , is now  $\varphi_{RL}(\varepsilon, r_R) Y_L(\hat{r}_R)$  inside its own sphere and for its own angular momentum, it is  $\psi_{RL}(\varepsilon, \mathbf{r})$  in the interstitial region, and inside the sphere at  $\mathbf{R}'$ , it vanishes for any other ( $R'L' \neq RL$ ) active channel, but is proportional to  $\varphi_{R'L'}(\varepsilon, r_{R'}) Y_{L'}(\hat{r}_{R'})$  for an inactive channel. As a result, with the normalization  $\varphi_{RL}(\varepsilon, a_R) \equiv 1$ , the kinked partial wave is a continuous solution of Schrödinger's equation with energy  $\varepsilon$ . But since it has kinks at the spheres in the active channels, it is *not* a wave function.

The solid curve in the left-hand part of Fig. 3 shows the Si  $p_{x=y=z}$  kinked partial wave for  $\varepsilon$  in the middle of the valence band and for  $\mathbf{r}$  along the  $[111]$ -line in the diamond structure from the central Si atom, through the nearest Si neighbor, and half-way into the back-bond void. The other curves will be explained when we come to consider potential overlap. The kinks at the  $a$ -spheres (chosen smaller than touching) are clearly seen. Since this kinked partial wave is designed for use in a minimal  $sp^3$ -basis, only the Si  $s$  and  $p$  waves were chosen as active. The inactive waves must therefore be provided by the tails of the kinked partial waves centered at the neighbors, and this is the reason for the strong Si  $d$ -character seen inside the nearest-neighbor sphere. Had we been willing to keep Si  $d$ -orbitals in the basis, the Si  $d$ -channels would have been active so that only waves with  $l > 2$  would have remained inside the neighbor spheres, whereby the kinked partial wave would have been more localized. Hence, the price for a smaller kinked-partial wave basis, is longer spatial range and a stronger energy dependence.

The element  $K_{R'L', RL}(\varepsilon)$  of the Hermitian *kink matrix* is defined as the kink of  $\phi_{RL}(\varepsilon, \mathbf{r})$  at the  $a_{R'}$ -sphere, projected onto  $Y_{L'}(\hat{r}_{R'})/a_{R'}^2$ . Hence, it specifies how the Hamiltonian operates on the set of kinked partial waves:

$$\begin{aligned}
(\mathcal{H} - \varepsilon) \phi_{RL}(\varepsilon, \mathbf{r}) &\equiv [-\Delta + V(\mathbf{r}) - \varepsilon] \phi_{RL}(\varepsilon, \mathbf{r}) = \\
&= - \sum_{R'L'} \delta(r_{R'} - a_{R'}) Y_{L'}(\hat{r}_{R'}) K_{R'L',RL}(\varepsilon).
\end{aligned} \tag{2}$$

Although an individual kinked partial wave is not a wave function, any *smooth* linear combination,  $\sum_{RL} \phi_{RL}(\varepsilon, \mathbf{r}) c_{RL,i}$ , is. Schrödinger's equation may therefore be formulated as the matching- or kink-cancellation condition:  $\sum_{RL} K_{R'L',RL}(\varepsilon_i) c_{RL,i} = 0$  for all  $R'L'$ , which is a set of homogeneous linear equations, equivalent with the KKR equations [9]. Here, the indices run only over active channels. Since the kink-matrix is expensive to compute, it is not efficient to find a one-electron energy from:  $\det|K(\varepsilon_i)| = 0$ , and then solve the linear equations for the corresponding  $c_{RL,i}$ . Rather, we construct a basis set,  $\chi^{(N)}(\mathbf{r})$ , with the property that it spans any wave function,  $\Psi_i(\mathbf{r})$ , with an energy  $\varepsilon_i$  in the neighborhood of  $N+1$  chosen energies,  $\varepsilon_0, \dots, \varepsilon_N$ , to within an error  $\propto (\varepsilon_i - \varepsilon_0) \dots (\varepsilon_i - \varepsilon_N)$ , and then solve the generalized eigenvalue problem,

$$\sum_{RL} \left\langle \chi_{R'L'}^{(N)} | \mathcal{H} - \varepsilon_i | \chi_{RL}^{(N)} \right\rangle b_{RL,i} = 0 \quad \text{for all } R'L', \tag{3}$$

resulting from the Raleigh-Ritz variational principle.

*MTOs.* – Since all wave functions with  $\varepsilon_i = \varepsilon$  may be expressed as:  $\sum_{RL} \phi_{RL}(\varepsilon, \mathbf{r}) c_{RL,i}$ , the MTOs with  $N=0$  are simply the kinked partial waves at the chosen energy:  $\chi_{RL}^{(0)}(\mathbf{r}) = \phi_{RL}(\varepsilon_0, \mathbf{r})$ . The Hamiltonian and overlap matrices are respectively  $\langle \chi^{(0)} | \mathcal{H} - \varepsilon_0 | \chi^{(0)} \rangle = -K(\varepsilon_0)$  and  $\langle \chi^{(0)} | \chi^{(0)} \rangle = \dot{K}(\varepsilon_0)$ , as may be found from Eq. (2) and the normalization chosen. Here,  $\dot{\phantom{x}} \equiv \partial/\partial\varepsilon$ . In order to find the MTOs with  $N>0$ , we first define a *Green matrix*:  $G(\varepsilon) \equiv K(\varepsilon)^{-1}$ , and then, by an equation of the usual type:  $(\mathcal{H} - \varepsilon) \gamma_{RL}(\varepsilon, \mathbf{r}) = -\delta(r_R - a_R) Y_L(\hat{r}_R)$ , a Green function,  $\gamma_{RL}(\varepsilon, \mathbf{r})$ , which has one of its spatial variables confined to the  $a$ -spheres, *i.e.*  $\mathbf{r}' \rightarrow RL$ . Considered a function of  $\mathbf{r}$ , this confined Green function is a solution with energy  $\varepsilon$  of the Schrödinger equation, except at its own sphere and for its own angular momentum, where it has a kink of size unity. This kink becomes negligible when  $\varepsilon$  is close to a one-electron energy, because the Green function has a pole there. Eq. (2) shows that  $\gamma(\varepsilon, \mathbf{r}) = \phi(\varepsilon, \mathbf{r}) G(\varepsilon)$ . (Here and in the following, lower-case letters, such as  $\gamma$  and  $\phi$ , denote vectors, and upper-case letters, such as  $K$  and

$G$ , denote matrices;  $\varepsilon$ ,  $\epsilon$ ,  $RL$ , and  $N$  are numbers, though). The confined Green function is thus factorized into a Green matrix  $G(\varepsilon)$  which has the full energy dependence, and a vector of functions  $\phi(\varepsilon, \mathbf{r})$  which has the full spatial dependence and a weak energy dependence. (The energy windows we consider are limited in size by the requirement that  $\phi_{RL}(\varepsilon, \mathbf{r})$  and  $\phi_{RL}(\varepsilon', \mathbf{r})$  cannot be orthogonal). Finally, we want to factorize the  $\mathbf{r}$  and  $\varepsilon$ -dependences completely and, hence, to approximate the confined Green function by  $\chi^{(N)}(\mathbf{r}) G(\varepsilon)$ : We note that subtracting from the Green function a function which is analytical in energy,  $\phi(\varepsilon, \mathbf{r}) G(\varepsilon) - \omega^{(N)}(\varepsilon, \mathbf{r}) \equiv \chi^{(N)}(\varepsilon, \mathbf{r}) G(\varepsilon)$ , produces an equally good Green function in the sense that both yield the same Schrödinger-equation solutions. If we can therefore determine the vector of analytical functions,  $\omega^{(N)}(\varepsilon, \mathbf{r})$ , in such a way that each  $\chi_{RL}^{(N)}(\varepsilon, \mathbf{r})$  takes the *same* value,  $\chi_{RL}^{(N)}(\mathbf{r})$ , at all mesh points, then  $\chi_{RL}^{(N)}(\varepsilon, \mathbf{r}) = \chi_{RL}^{(N)}(\mathbf{r}) + O((\varepsilon - \epsilon_0) \dots (\varepsilon - \epsilon_N))$ . Hence,  $\chi^{(N)}(\mathbf{r})$  is the set of NMTOs. Now, since  $\chi^{(N)}(\epsilon_0, \mathbf{r}) = \dots = \chi^{(N)}(\epsilon_N, \mathbf{r})$ , the  $N$ th divided difference of  $\chi^{(N)}(\varepsilon, \mathbf{r}) G(\varepsilon)$  equals  $\chi^{(N)}(\mathbf{r})$  times the  $N$ th divided difference of  $G(\varepsilon)$ . Moreover, if we let  $\omega^{(N)}(\varepsilon, \mathbf{r})$  be a polynomial in energy of  $(N-1)$ st degree, its  $N$ th divided difference on the mesh,  $\Delta^N \omega^{(N)}(\mathbf{r}) / \Delta[0 \dots N]$ , will vanish. We have therefore found the following solution:

$$\chi^{(N)}(\mathbf{r}) = \frac{\Delta^N \phi(\mathbf{r}) G}{\Delta[0 \dots N]} \left[ \frac{\Delta^N G}{\Delta[0 \dots N]} \right]^{-1} \quad (4)$$

$$\begin{aligned} &\equiv \phi(\epsilon_N, \mathbf{r}) + \frac{\Delta \phi(\mathbf{r})}{\Delta[N-1, N]} (E^{(N)} - \epsilon_N) + \dots \\ &\dots + \frac{\Delta^N \phi(\mathbf{r})}{\Delta[0 \dots N]} (E^{(1)} - \epsilon_1) \dots (E^{(N)} - \epsilon_N), \end{aligned} \quad (5)$$

for the NMTO set. Since the kinks,  $(\mathcal{H} - \varepsilon) \phi(\varepsilon, \mathbf{r}) G(\varepsilon)$ , are independent of  $\varepsilon$ , NMTOs with  $N > 0$  are smooth. By use of the well-known expression for a divided difference:

$$\frac{\Delta^N \phi(\mathbf{r}) G}{\Delta[0 \dots N]} = \sum_{n=0}^N \frac{\phi(\epsilon_n, \mathbf{r}) G(\epsilon_n)}{\prod_{m=0, \neq n}^N (\epsilon_n - \epsilon_m)},$$

we finally obtain the expressions for the Lagrange matrices in Eq. (1) and the energy matrices in Eq. (5):  $E^{(M)} = (\Delta^M \varepsilon G / \Delta[0 \dots M]) (\Delta^M G / \Delta[0 \dots M])^{-1}$ , in terms of the values of the Green matrix on the energy mesh.

The NMTO set may thus be thought of as a 'quantized' Lagrange interpolation of the kinked partial-wave set, where the weights are matrices rather than  $N$ th-degree scalar polynomials in energy. Similarly, Eq. (5) may be interpreted as a 'quantized' Newton interpolation with the energies substituted by matrices. If the mesh is condensed, Newton interpolation becomes Taylor expansion:  $\Delta^N \phi / \Delta [0 \dots N] \rightarrow (1/N!) d^N \phi / d\varepsilon^N$ . The form (5) expresses the NMTO as a kinked partial wave at the same site and with the same angular momentum, plus a smoothing cloud of energy-derivative functions centered at all sites and with all angular momenta. In the right-hand part of Fig. 3, the solid curve is the MTO with  $N=1$ , and the dashed curve is the MTO with  $N=0$  shown also in the left-hand part. Here again, longer spatial range is the price for spanning the wave functions in a wider energy range. The increase of range and smoothness with  $N$  follows from the relation:  $(\mathcal{H} - \epsilon_N) \chi^{(N)}(\mathbf{r}) = \chi^{(N-1)}(\mathbf{r}) (E^{(N)} - \epsilon_N)$ , which also shows that the  $E$ 's are transfer matrices between MTO sets of different order. Linear transformations of the kinked partial waves,  $\hat{\phi}(\varepsilon, \mathbf{r}) = \phi(\varepsilon, \mathbf{r}) \hat{T}(\varepsilon)$ , change the NMTOs, but not the Hilbert space spanned by them [1]. This may be used to generate nearly orthonormal representations where the  $\hat{E}$ 's are Hamiltonians and where  $\langle \hat{\chi}^{(M-1)} | \hat{\chi}^{(M)} \rangle \equiv 1$  for  $1 \leq M \leq N$ .

The expressions for the Hamiltonian and overlap matrices needed in (3) may be worked out and given as [1]:

$$\frac{\Delta^N G}{\Delta [0 \dots N]} \langle \chi^{(N)} | \varepsilon - \mathcal{H} | \chi^{(N)} \rangle \frac{\Delta^N G}{\Delta [0 \dots N]} = \frac{\Delta^{2N} G}{\Delta [[0 \dots N-1] N]} + (\varepsilon - \epsilon_N) \frac{\Delta^{2N+1} G}{\Delta [[0 \dots N]]}. \quad (6)$$

$\Delta^{M+N+1} G / \Delta [[0 \dots M] N]$  is the  $(M+N+1)$ st derivative of that polynomial of degree  $M+N+1$  which takes the values  $G(\epsilon_0), \dots, G(\epsilon_N)$  at the  $N+1$  mesh points and, at the first  $M+1$  points, also the values  $\dot{G}(\epsilon_0), \dots, \dot{G}(\epsilon_M)$  of the energy-derivatives. The one-electron energies are 'ratios' of energy derivatives of such 'Hermite interpolations' of  $G(\varepsilon)$ , which itself has poles inside the mesh.

Having seen that the formalism is expressed in terms of *one* matrix, *e.g.*  $K(\varepsilon) = \langle \chi^{(0)} | \varepsilon - \mathcal{H} | \chi^{(0)} \rangle = G(\varepsilon)^{-1}$ , let us indicate how this

is generated [5,10]: The elements of the *bare* KKR structure matrix [9],  $B_{R'L',RL}^0(\varepsilon) \equiv \sum_{l''} 4\pi i^{-l+l'-l''} C_{LL'l''} \kappa n_{l''}(\kappa|\mathbf{R}-\mathbf{R}'|) Y_{L''}^* \left( \widehat{\mathbf{R}-\mathbf{R}'} \right)$  for  $R \neq R'$ , and  $\equiv 0$  for  $R=R'$ , specify how the spherical waves,  $n_l(\kappa r_R) Y_L(\hat{r}_R)$ , are expanded in regular spherical waves,  $j_{l'}(\kappa r_{R'}) Y_{L'}(\hat{r}_{R'})$ . The corresponding expansions of the screened spherical waves are now specified by a screened structure matrix, defined via:  $B^\alpha(\varepsilon)^{-1} \equiv B^0(\varepsilon)^{-1} + \kappa^{-1} \tan \alpha(\varepsilon)$ , and obtained by matrix inversion of  $B^0(\varepsilon) + \kappa \cot \alpha(\varepsilon)$ . Here,  $\kappa \cot \alpha(\varepsilon)$  is a diagonal matrix with  $\alpha_{RL}(\varepsilon)$  being the hard-sphere phase shift,  $\tan \alpha_{RL}(\varepsilon) \equiv j_l(\kappa a_R) / n_l(\kappa a_R)$ , if the channel is active, and the true phase shift,  $\eta_{RL}(\varepsilon)$ , if the channel is inactive.  $B^\alpha(\varepsilon)$  has short spatial range for energies well below the 'hard-sphere continuum,' as defined by the division into active and inactive channels and the choice of  $a$ -radii for the former. The kink matrix is finally:  $K(\varepsilon) = -[\kappa n(\kappa a)]^{-1} [B^\alpha(\varepsilon) + \kappa \cot \eta^\alpha(\varepsilon)] [\kappa n(\kappa a)]^{-1}$ , where  $\eta^\alpha(\varepsilon)$  is the phase shift in the medium of hard  $a$ -spheres:  $\tan \eta^\alpha(\varepsilon) \equiv \tan \eta(\varepsilon) - \tan \alpha(\varepsilon)$ .  $B^\alpha(\varepsilon)$  contains the essence of the hopping integrals, whose dependence on the local environment enters through the screening.

When the potentials overlap, we need to redefine the kinked partial waves as illustrated in Fig. 3:  $\phi_{RL}(\varepsilon, \mathbf{r}) \equiv [\varphi_{RL}(\varepsilon, r_R) - \varphi_{RL}^o(\varepsilon, r_R)] Y_L(\hat{r}_R) + \psi_{RL}(\varepsilon, \mathbf{r})$ . Here,  $\varphi(\varepsilon, r)$  (dot-dashed) is the radial solution for the central MT-well, which now extends to  $s(>a)$ .  $\varphi^o(\varepsilon, r)$  (dotted) is the phase-shifted wave proceeding smoothly inwards from  $s$  to the central  $a$ -sphere, where it is matched with a kink to the screened spherical wave  $\psi$  (dashed). It is easily shown that, with this modification, the formalism holds to first order in the potential-overlap [1,5,10]. In practice, this means that radial overlaps of up to 30% may be treated without changes, and that overlaps as large as in Fig. 3, may be treated by adding a simple kinetic-energy correction [1,5,10,11]. This should make the use of empty spheres superfluous and open the way for efficient DF-molecular-dynamics calculations. The  $a$ -radii now specify the screening, with a default value which is 80% of the atomic or ionic radius, and for semi-core states, the core radius.

In conclusion, we have solved the long-standing problem of deriving useful, minimal sets of short-ranged orbitals from scattering theory. Into a calculation enters: (1) The phase

shifts of the potential wells. (2) A choice of which orbitals to include in the set, the so-called active channels. (3) For these, a choice of screening radii,  $a_{RL}$ , to control the orbital ranges. (4) An energy mesh on which the set will provide exact solutions. These MTOs have significant advantages over those used in the past.

## REFERENCES

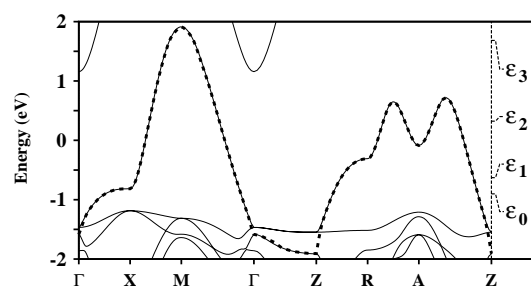
- [1] A complete account of the present work is included in the article by O.K. Andersen *et al.* in [2].
- [2] *Electronic Structure and Physical Properties of Solids. The Uses of the LMTO Method*, Ed. H. Dreyse (Springer Lecture Notes in Physics, New York, 2000).
- [3] T.F.A. Müller *et al.*, Phys. Rev. B **57**, R12655 (1998).
- [4] O.K. Andersen *et al.*, Phys. Rev. Lett. **53**, 2571 (1984).
- [5] O.K. Andersen *et al.* in *Methods of Electronic Structure Calculations*, Eds. V. Kumar *et al.* (World Scientific, Singapore, 1994), pp. 63-124; and in [6] pp. 3-34; R.W. Tank and C. Arcangeli, phys. stat. sol. (b) **217**, 89 (2000).
- [6] *Tight-Binding Approach to Computational Materials Science*, Eds. P.E.A. Turchi, A. Gonis, and L. Colombo, Symp. Proc. Vol. 491 (Mat. Res. Soc., Pittsburgh, 1998).
- [7] F. Aryasetiawan *et al.*, Rep. Prog. Phys. **61**, 237 (1998).
- [8] R. Zeller *et al.*, Phys. Rev. B **52**, 8807 (1995).
- [9] *Applications of Multiple Scattering Theory to Materials Science*, Eds. W.H. Butler *et al.*, Symp. Proc. Vol. 253 (Mat. Res. Soc., Pittsburgh, 1992).
- [10] O.K. Andersen, A.V. Postnikov, S.Y. Savrasov in [9].
- [11] C. Arcangeli and O.K. Andersen (unpublished).

## FIGURES

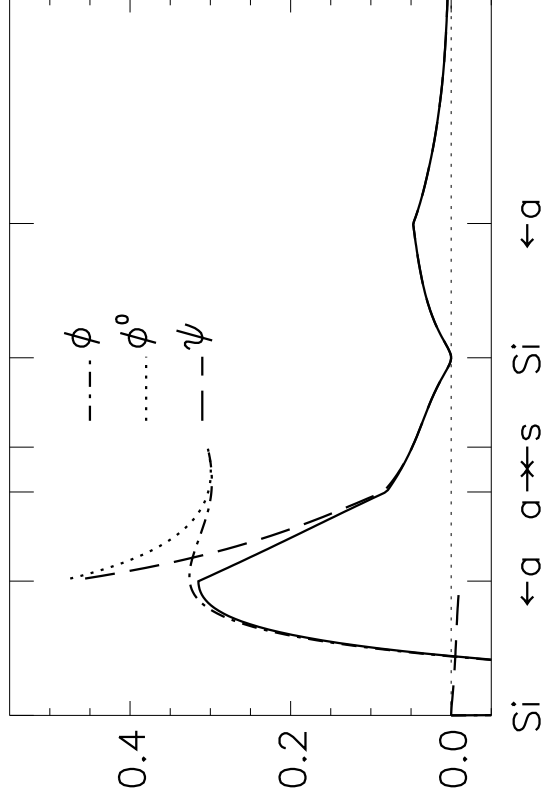
FIG. 1. The Cu  $d_{x^2-y^2}$ -like LMTO, which describes the (LDA) conduction band of  $\text{HgBa}_2\text{CuO}_4$ , plotted in the  $\text{CuO}_2$  plane. Cu and O sites are marked by respectively + and \*.

FIG. 2. Band structure of  $\text{CaCuO}_2$  with a  $7^0$ -buckle, calculated in the LDA with a single Bloch Cu  $d_{x^2-y^2}$  CMTO (dotted) compared with the full band structure (solid).

FIG. 3. Si  $p_{x=y=z}$  kinked partial wave (KPW), its constituents  $\varphi, \varphi^o$ , and  $\psi$ , and the LMTO. No empty spheres were used.  $s$  is the range of the central potential well.



Si p kinked partial wave



Si p Imto

